Multiphonon Raman and infrared spectra of isotopically controlled diamond

R. Vogelgesang, A. D. Alvarenga, Hyunjung Kim, A. K. Ramdas, and S. Rodriguez
Department of Physics, Purdue University, West Lafayette, Indiana 47907

M. Grimsditch
Argonne National Laboratory, Argonne, Illinois 60439

T. R. Anthony
GE Corporate Research and Development, Schenectady, New York 12309
(Received 3 February 1998; revised manuscript received 13 May 1998)

Two-phonon spectra of $^{12}C_{1-x}{}^{13}C_x$ diamonds, $0 \leqslant x \leqslant 1$, are measured with a sensitive charge-coupled device-based Raman and a Fourier transform infrared spectrometer. Exploiting the infrared activity and the polarization characteristics of the Raman spectra recorded for a variety of scattering geometries, the two-phonon features are interpreted in terms of the critical points revealed in the phonon dispersion curves determined by inelastic neutron scattering. The occurrence of identical spectroscopic features in both ^{13}C and natural diamond, consistent with virtual crystal approximation, proved invaluable in arriving at assignments for them. Space group selection rules for two-phonon combinations/overtones and the wave-vector conservation, all employed in a self-consistent fashion, yield the frequencies of the critical points with improved precision. [S0163-1829(98)04333-1]

I. INTRODUCTION

As is well known, inelastic neutron scattering of monoenergetic neutrons from a single crystal, measured as a function of crystallographic orientation, in principle allows one to deduce the *complete* dispersion curve of lattice vibrations, i.e., $\omega(\mathbf{q})$, where ω is the frequency and $\mathbf{q}$ the wave vector of the phonon.[1] In contrast, spectroscopic techniques yield information only about *specific* parts of the Brillouin zone (BZ), but the frequencies of the vibrational modes accessible in infrared (IR), Raman and/or Brillouin spectroscopy are determined with significantly superior precision.[2,3] It should be emphasized that the inelastic neutron-scattering technique needs large single crystals; Warren, Wenzel, and Yarnell[1,4] for instance, used two extraordinarily large (one 242.8 carat and the other 253.7 carat) natural diamonds in their classic work on the phonon dispersion curves. The cost and effort of growing an isotopically controlled diamond of such size are inconceivable with the current crystal growth techniques.

The precision accessible in spectroscopy, together with the space group selection rules that predict IR and Raman activity (including polarization characteristics) of overtones/combinations, enable one to derive $\omega(\mathbf{q})$ at specific points of the BZ in addition to the zone center. In such an analysis, inelastic neutron-scattering data provide an indispensable starting point. This was indeed the approach adopted by Solin and Ramdas[5] in their analysis of the second-order Raman spectrum of natural diamond (98.9% ^{12}C and 1.1% ^{13}C).

The larger shift (by a factor of approximately 2) in the second-order Raman spectra compared to that of the $\Gamma^{(25+)}$ first-order Raman mode provides a motivation for the study of the two-phonon Raman and IR spectra of isotopically controlled diamond[6] as a function of their composition $^{12}C_{1-x}{}^{13}C_x$, where $0 \leqslant x \leqslant 1$. In particular, precise information about the isotopic effects in the dispersion curves of diamond, following an approach similar to that adopted in Ref. 5, and the effects related to isotopic order/disorder, are additional reasons for such a study.

II. THEORETICAL CONSIDERATIONS: SELECTION RULES

Raman and Brillouin scattering with visible laser sources and absorption in the IR involve electromagnetic radiation with wavelengths (λ) much larger than the lattice constant a; thanks to the translational symmetry of the crystal, or equivalently wave-vector conservation, the creation and annihilation of a single quantum of lattice vibration are then possible for phonons with wave vectors $\mathbf{q} \sim 0$, i.e., near the center of the BZ. Conservation of energy leads to $\hbar\omega$(scattered photon)$=\hbar\omega$(laser)$\pm\hbar\omega$(phonon) in Raman/Brillouin scattering and $\hbar\omega$(incident photon)$=\hbar\omega$(phonon) in IR absorption. In addition, the corresponding lattice vibrations also need to produce an oscillatory change in polarizability to be Raman active or in electric dipole moment to be IR active. A factor group analysis[2] of the zone-center optical phonons yields the so-called rule of mutual exclusion for crystal structures with inversion symmetry, as in the diamond structure characteristic of the group IV elements; for this structure the zone-center optical phonon is Raman active and IR inactive.[7] Note that Brillouin scattering, viewed as Bragg scattering from the optical stratifications generated by long-wavelength acoustic lattice vibrations, arises from the associated elasto-optic effects and is observed in all crystals; the Doppler shifts produced by the moving ''Bragg'' planes yield the velocity of sound and, hence, the combinations of elastic moduli characteristic of the relevant acoustic phonons.

For Raman and IR multiphonon processes, periodicity of the perfect crystal also imposes the selection rules $\Sigma_j \pm \mathbf{q}_j$

TABLE I. Phonon frequencies at critical and high-symmetry points of the phonon dispersion curves. The representations of the associated phonon(s) are indicated in the notation of Birman (Refs. 10 and 11) along with their nature (O=optical, A=acoustic, L=longitudinal, T=transverse). The phonon frequencies as determined in the present study are given in the last column with errors of $\pm 2\ \mathrm{cm}^{-1}$, except where stated differently. (See the text for a discussion of the Σ line.)

		Frequency (cm^{-1})		
q ($2\pi/a$)	Representation	Neutron (Refs. 1 and 4)	Ref. 5	Present study
Γ: (0,0,0)	$\Gamma^{(15-)}$ (A)			0.0 ± 0.0
	$\Gamma^{(25+)}$ (O)		1332	1332.4 ± 0.01
L: $(\frac{1}{2},\frac{1}{2},\frac{1}{2})$	$L^{(3-)}$ (TO)	1210 ± 37	1206	1208
	$L^{(2-)}$ (LO)	1242 ± 37	1252	1245
	$L^{(1+)}$ (LA)	1035 ± 32	1006	1009
	$L^{(3+)}$ (TA)	552 ± 16	563	572
X: (1,0,0)	$X^{(1)}$ (L)	1184 ± 21	1185	1170
	$X^{(3)}$ (TA)	807 ± 32	807	786
	$X^{(4)}$ (TO)	1072 ± 26	1069	1088
W: $(1,\frac{1}{2},0)$	$W^{(1)}$ (TO)	993 ± 53	999	1012
	$W^{(2)}$ (L)	1168 ± 53	1179	1164
	$W^{(2)}$ (TA)	918 ± 11	908	915
Σ: $(\xi,\xi,0)$	$\Sigma^{(1)}$ (O)	1231 ± 32	1230	1236
	$\Sigma^{(2)}$ (O)	1120 ± 21	1109	1112
$\xi\sim 0.72$	$\Sigma^{(3)}$ (O)	1046 ± 21	1045	1051
	$\Sigma^{(1)}$ (A)	982 ± 11	988	986
	$\Sigma^{(3)}$ (A)	993 ± 16	980	982
	$\Sigma^{(4)}$ (A)	748 ± 16		748

$=\mathbf{k}_i-\mathbf{k}_s$ and $\Sigma_j \pm \mathbf{q}_j=\mathbf{k}_i$, respectively. Here $\mathbf{k}_i$ and $\mathbf{k}_s$ are the incident and the scattered photon wave vectors, respectively, and $\mathbf{q}_j$ are the wave vectors of the phonons involved, the associated signs referring to phonon creation (+) or annihilation (−). Since $\mathbf{k}_i-\mathbf{k}_s\sim 0$ for Raman and $\mathbf{k}_i\sim 0$ for IR processes, the generalized wave-vector conservation is

$$\sum_j \pm \mathbf{q}_j \sim 0, \tag{1}$$

with conservation of energy being ensured in the multiphonon excitation and deexcitation. Given the magnitude of the critical point frequencies in diamond, it is realistic to restrict the discussion to phonon creation. In second-order processes, it is thus clear that $\mathbf{q}\simeq -\mathbf{q}'$; the symmetry of the phonon dispersion curves in diamond in turn allows the combinations and overtones to occur between phonon branches at a given **q**. Assuming absorption and scattering cross sections are smooth functions of frequency and frequency shift, respectively, the second-order IR or Raman spectra are quasicontinuous in nature, reflecting the two-phonon joint density of states along with its peaks and slope discontinuities. The peaks and slope discontinuities occur, consistent with wave-vector conservation, at the *critical points* (CP's) in the joint density of states given by

$$\nabla_{\mathbf{q}}(\omega_{\sigma,\mathbf{q}}+\omega_{\sigma',\mathbf{q}})=0, \tag{2}$$

where σ and σ' are the phonon branch indices (note that $\omega_{\sigma,-\mathbf{q}}=\omega_{\sigma,\mathbf{q}}$). One can visualize three cases: Case (i) $\nabla_{\mathbf{q}}(\omega_{\sigma,\mathbf{q}})=\nabla(\omega_{\sigma',\mathbf{q}})=0$, corresponding to the well-known van Hove singularities in each of the phonon branches.[8,9] Case (ii) overtone of a van Hove singularity in a given branch σ with $\nabla_{\mathbf{q}}(2\omega_{\sigma,\mathbf{q}})=0$. Such singularities definitely occur at high-symmetry points in the BZ, in diamond at Γ, *X*, *L*, and *W*. But CP's can also arise at a general **q** due to specific features of the lattice dynamics. Case (iii) new CP's not dictated by symmetry considerations but characterized by $\nabla_{\mathbf{q}}(\omega_{\sigma,\mathbf{q}})=-\nabla(\omega_{\sigma',\mathbf{q}})\neq 0$, i.e., with the two-phonon branches σ and σ' at a specific **q** but with opposite gradients. The Σ line provides examples of all three cases.

We follow Birman[10,11] in labeling the symmetries of the CP's and the irreducible representations according to which the normal coordinates, the polarizability tensor, and the polar vector transform in O_h^7 ($Fd\bar{3}2/m$), the space group of diamond. In Table I these CP's are listed along with the nature of the relevant phonons.

The electric-dipole operator in O_h transforms as a polar vector, i.e., according to $\Gamma^{(15-)}$. Hence, only those overtones or combinations are IR active, whose final states given by $[\Gamma_i]^{(2)}$ ($\sigma=\sigma'$) or $\Gamma_i\otimes\Gamma_j$ ($\sigma\neq\sigma'$), respectively, contain $\Gamma^{(15-)}$, *i* and *j* being the two phonons involved. Raman-scattering transitions are characterized by a symmetric, second-rank polarizability tensor, which in O_h transforms as

$$[\Gamma^{(15-)}]^{(2)}=\Gamma^{(1+)}+\Gamma^{(12+)}+\Gamma^{(25+)}. \tag{3}$$

Hence, only those overtones or combinations, whose product representations contain $\Gamma^{(1+)}$, $\Gamma^{(12+)}$, or $\Gamma^{(25+)}$ symmetry

TABLE II. The equivalent nomenclatures of Birman (B) (Refs. 10 and 11), Wilson, Decius, and Cross (WDC) (Ref. 12), Koster *et al.* (K) (Ref. 13), and Bouckaert, Smoluchowski, and Wigner (BSW) (Ref. 14).

B	WDC	K	BSW
$\Gamma^{(1+)}$	A_{1g}	Γ_1^+	Γ_1
$\Gamma^{(12+)}$	E_g	Γ_3^+	Γ_{12}
$\Gamma^{(25+)}$	$F_{2g} \equiv T_{2g}$	Γ_5^+	Γ'_{25}
$\Gamma^{(15-)}$	$F_{1u} \equiv T_{1u}$	Γ_4^-	Γ_{15}

are Raman active. Note that the zone-center optical phonon of diamond with $\Gamma^{(25+)}$ symmetry is Raman active and IR inactive. The corresponding *Raman tensors* $[\alpha_{ij}]$, referred to the cubic axes x,y,z, have the forms

$$\Gamma^{(1+)}: \quad \begin{bmatrix} a & 0 & 0 \\ 0 & a & 0 \\ 0 & 0 & a \end{bmatrix};$$

$$\Gamma^{(12+)}: \quad \begin{bmatrix} -b & 0 & 0 \\ 0 & -b & 0 \\ 0 & 0 & 2b \end{bmatrix}, \begin{bmatrix} \sqrt{3}b & 0 & 0 \\ 0 & -\sqrt{3}b & 0 \\ 0 & 0 & 0 \end{bmatrix};$$

$$\Gamma^{(25+)}: \quad \begin{bmatrix} 0 & 0 & 0 \\ 0 & 0 & d \\ 0 & d & 0 \end{bmatrix}, \begin{bmatrix} 0 & 0 & d \\ 0 & 0 & 0 \\ d & 0 & 0 \end{bmatrix}, \begin{bmatrix} 0 & d & 0 \\ d & 0 & 0 \\ 0 & 0 & 0 \end{bmatrix}. \quad (4)$$

With such tensors the scattering intensity for the two-phonon features can be readily deduced for any scattering geometry. For convenience, the various nomenclatures prevalent in the literature for the Raman and IR active irreducible representations are presented in Table II.[10–14]

III. EXPERIMENTAL PROCEDURE AND APPARATUS

A. Growth

In the present investigation we have studied natural as well as synthetic type-IIa diamonds,[15] the latter with an isotopic composition range $0 \leqslant x \leqslant 1$. As described elsewhere,[6] the synthesis of diamonds of small x involved the initial growth of thin diamond films of the desired isotopic composition by chemical vapor deposition (CVD),[16] which were pulverized and used as diamond feedstock in a high-pressure–high-temperature (HPHT) growth[17] of the gemstone. For samples containing significant amounts of ^{13}C carbon, isotopically controlled graphite, rather than CVD diamond, was used in the HPHT process, since graphite can be produced much more efficiently using a pyrolytic cracking process.[18]

B. Raman

Raman spectra were excited with the 4762 Å line from a Kr^+ laser (Spectra Physics Model 171).[19] A Babinet compensator was used to prepare the incident light with the desired linear polarization. All the experiments were performed at room temperature (~300 K) and in the backscattering geometry, normal to the desired crystallographic face. An adjustable sample mount allowed the crystal axes to be oriented in the desired scattering geometry. The inelastically scattered light was spectrally dispersed and analyzed with a Jobin/Yvon T-64000 triple monochromator.[20] The analyzer was set at $\pm 45°$ with respect to the rulings of the monochromator gratings, thus ensuring the same instrumental response to the two linear polarizations used for the analysis of the scattered beam. At the exit of the monochromator, a charge-coupled device (CCD) camera with 1024 channels recorded the spectral images, with an instrumental resolution of 4 cm^{-1}. The spectra were calibrated individually to an accuracy better than 0.2 cm^{-1}, using reference lines from a UVP PenRay[21] low-pressure Ne discharge lamp. In order to compensate for the channel-by-channel variation in the detector sensitivity, the spectrum of white light from a tungsten lamp was recorded and fitted to a linear function representative of the small spectral range covered; the ratio of this fit to the actual readouts provided the necessary channel compensation factors, applied to every raw spectrum prior to further processing. A complete Raman spectrum, extending from approximately 300 to 3300 cm^{-1}, was generated by recording six different, overlapping spectral patches and matching them numerically.

C. Fourier transform IR (FTIR)

The absorption spectra of IR-active second-order features were obtained with a BOMEM DA 3 Fourier transform spectrometer,[22] employing a Globar source, a KBr beamsplitter and a liquid-nitrogen-cooled mercury-cadmium-telluride detector. Spectra recorded with 1.0 cm^{-1} resolution proved more than adequate in view of the linewidths of the spectral features.

IV. EXPERIMENTAL RESULTS AND DISCUSSION

A. Natural composition

Figure 1 shows the room-temperature IR absorption spectrum of a type-IIa natural diamond. The spectrum is characterized by the absence of the $\Gamma^{(25+)}$, zone-center optical mode occurring at $\omega_0 = 1332.4\ cm^{-1}$ for natural diamond. (See inset to the figure.) The room-temperature Raman spectrum of a natural type-IIa diamond displayed in Fig. 2 shows the intense Raman-allowed first-order line at ω_0 as well as the significantly weaker quasicontinuous multiphonon features (see inset). The positions of the peaks and slope discontinuities characterizing the multiphonon IR and Raman spectra are listed in Table III.

We specify the scattering geometry using the standard convention,[23] viz., $i(jk)l$, where i is the incident direction; j, the incident polarization; k, the scattered polarization; and l, the scattered direction. In Fig. 3, we present some of the spectra for the same sample recorded in backscattering along $x \| [100]$ in which the incident and scattered polarization is along $y \| [010]$ or $z \| [001]$, or along $y' \| [011]$ or $z' \| [0\bar{1}1]$.

B. Analysis procedure

The two-phonon features are identified as combinations and overtones of the CP phonons consistent with (1) conservation of wave vector, (2) the frequency range compatible with error bars in the neutron data, and (3) selection rules for

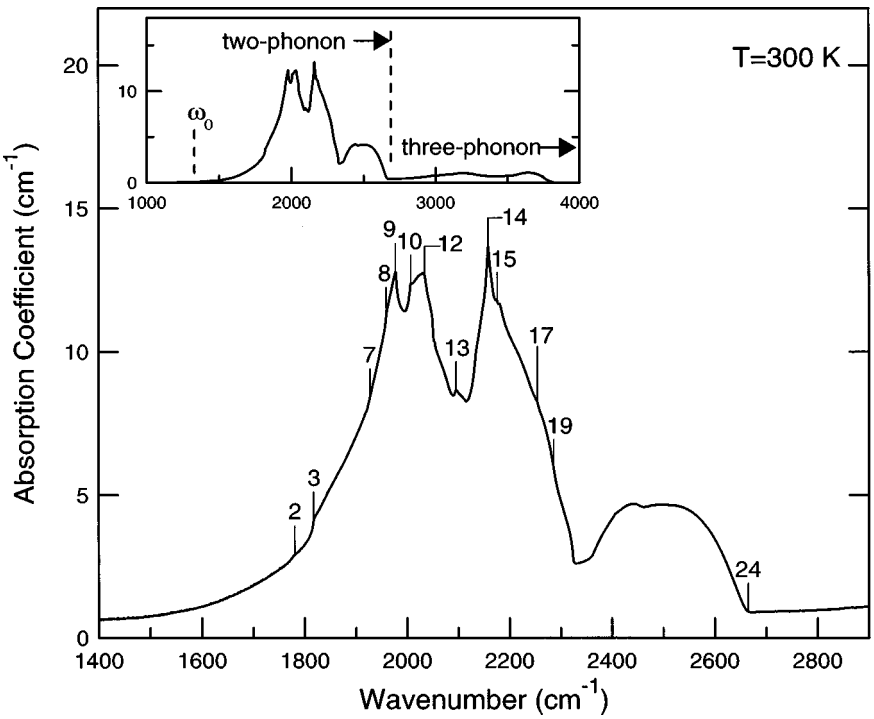

FIG. 1. The room temperature IR absorption spectrum of a natural type-IIa diamond (specimen $D4$). The two-phonon features identified in Table III are explicitly labeled. The inset covering a larger spectral range also shows the three-phonon features as well as the *absence* of the $\Gamma^{(25+)}$ zone center optical phonon.

IR and Raman activity predicted by group-theoretical considerations. One must bear in mind that the group-theoretical prediction for the activity of an overtone or a combination is a necessary but not a sufficient condition, since a given feature may be too weak to be observed or may be obscured by a strong underlying continuum.

Table I displays the frequencies of the CP phonons (along with the associated error bars) as deduced from inelastic neutron scattering.[1,4] On the basis of these frequencies, one can generate a list of overtones/combinations *consistent with the conservation of wave vector*. At this stage the prominent features in the two-phonon IR and Raman spectra are identified as possible candidates compatible with the frequencies (together with the combined error brackets) of the neutron data on the one hand and the group-theoretical selection rules, predicting IR *activity as well as polarization features in the Raman spectra* on the other hand. Among the multiple choices thus generated for a given spectral feature, a specific selection is now made in order to provide unique assignments for all the prominent features (i.e., Nos. 2, 3, 9–11, 13, 14, 17, 18, 20, 21, and 23 in Table III). The predictions based on such a selection of CP frequencies are tested with respect to further, less prominent spectral features and the selection rules they must obey. Alternate assignments for the prominent features are evaluated in the context of the maximum number of assignments within the significantly smaller error brackets in the IR and Raman spectra.

In order to identify spectral features in the Raman and IR spectra with the CP's that occur on the Σ line (ξ, ξ, 0), one must recognize that symmetry considerations do not provide a guide; it is necessary to discover them from the phonon dispersion curves as revealed in inelastic neutron scattering. The inspection of the neutron data show clear evidence of CP's at $\xi \sim 0.72$ for the $\Sigma^{(3)}$(O) and the $\Sigma^{(3)}$(A) single-phonon dispersion curves. From a polynomial least-squares fit to the single-phonon dispersion curve with the range $\xi = 0.2$ to 1.0, additional CP's can be identified at $\xi \sim 0.7$ and 0.5 for the $\Sigma^{(1)}$(O) branch. The occurrence of CP's in the two-phonon density of states arising from $\nabla_{\mathbf{q}}(\omega_{\sigma,\mathbf{q}}) = -\nabla_{\mathbf{q}}(\omega_{\sigma',\mathbf{q}}) \neq 0$ [Case (iii)], were established from polynomial fits to all the Σ branches. An inspection of the neutron dispersion curves showed that it was sufficient to explore the range $\xi = 0.65$ to 0.85 in this fashion. Phonon combinations interpreted in this manner are listed in Table III for $\xi \sim 0.7$, 0.75, 0.78, and 0.84. Once again, features in the Raman and IR spectra were identified, which are consistent with these CP's within the accuracy of the neutron data. In Table I we list the values of Σ phonons at $\xi = 0.72$, as derived from the polynomial fits used in the above assignments.

Noting that overtones are forbidden in the IR and circumscribed by the nature of the dispersion curves, one can deduce that no IR feature can occur at frequencies $> 2\omega_0$, the upper frequency limit for combinations of phonons of different branches at the same **q**. On this basis, the feature labeled ''24'' at 2665 cm^{-1} in Fig. 1 can be convincingly attributed to precisely such a limit. By the same token, only overtones, being Raman active, can be observed in the second-order Raman spectrum beyond 2665 cm^{-1}; the 2667 cm^{-1} sharp line (No. 25) is one of them. Thus the feature labeled ''27'' at 2690 cm^{-1} in Fig. 2 can be attributed to the high-frequency limit of the overtones, possibly the absolute maximum ($\omega_{\max}$) of the phonon dispersion curves including effects of overbending. (See also the remark in Ref. 24.) Between 2667 cm^{-1} and $2\omega_{\max}$, there is evidence of structure, e.g., the change of slope at 2676 cm^{-1} (No. 26). Overtones of the overbending maxima present in the calculation of Windl *et al.*[25] in the $\Lambda^{(1)}$(LO) and $\Delta'^{(2)}$(LO) branches,

as well as the saddle point on the $\Sigma^{(3)}$(O) branch, can well provide an explanation for this range.

C. Brout sum

In the harmonic approximation, the trace of the dynamical matrix is given by the Brout sum[26] $S(\mathbf{q})=\Sigma_\sigma \omega^2_{\sigma,\mathbf{q}}$ over all branches σ for a specific wave vector $\mathbf{q}$. It is constant with $\mathbf{q}$ for most kinds of interatomic forces, such as all electrostatic forces and/or forces between ''unlike'' atoms (i.e., those located at nonequivalent sites). As Rosenstock[27] has shown, if any of the forces does contribute variable terms to the trace, the systematic variation with $\mathbf{q}$ allows one to identify the relative location of the interacting atoms. In diamond, nonelectrostatic, central next-nearest-neighbor forces have been associated with the observed $\mathbf{q}$ dependence of $S(\mathbf{q})$.[27,28] In the notation of Rosenstock, these forces give

$$S(\mathbf{q})=S(\Gamma)+\beta_1(3-c_1c_2-c_2c_3-c_3c_1), \qquad (5)$$

where $c_i=\cos(q_ia/2)$. In the last column of Table IV we display the results of this simple model, using for the fitting parameter β_1 the value 0.2671×10^6 cm^{-2}. The good agreement of the model with observation can be convincingly visualized by comparing the nature of the lattice vibrations with wave vectors near the zone center vs those at the zone boundary. Whereas, in the former, the two fcc sublattices vibrate as rigid units against each other, leaving next-nearest-neighbor atoms fixed in their relative positions, the latter vibrations do exhibit relative motion of next-nearest neighbors. Thus, as one moves away from the zone center, interaction between next-nearest neighbors becomes increasingly important. In contrast to diamond, the Brout sums for silicon and germanium are essentially constant throughout the BZ (see Fig. 7 in Ref. 29).

D. Overbending

One of the significant features (No. 25) in the second-order Raman spectrum of diamond is the sharp line at 2667 cm^{-1} in natural specimens. As shown by Solin and Ramdas,[5] it is an intrinsic feature with predominantly $\Gamma^{(1+)}$ polarization characteristics and a frequency $\sim$2 cm^{-1} above twice ω_0. Its observation, independent of the laser excitation energy ($\hbar\omega_L<$*energy gap*), demonstrates that its occurrence cannot be associated with a resonance enhancement arising from an interband electronic transition.[30] It is also significant that the electric field induced changes in the two-phonon IR absorption spectrum—a technique that reproduces essentially the ''Raman'' spectrum—clearly shows this sharp feature;[31] so does the second-order Raman spectrum studied by Eesley and Levenson[32] with Raman induced Kerr-Effect spectroscopy.

A variety of mechanisms for the origins of the ($2\omega_0$ +2 cm^{-1}) feature of the second-order spectrum have been proposed and discussed;[24,25,33–40] of these, the interpretation of the 2667 cm^{-1} line as a consequence of an overbending in the topmost optical phonon dispersion near Γ, giving rise to a sharp maximum in the single-phonon density of states, appears most justifiable. Its frequency is in the range *above* that of the CP at Γ and below that of the additional overbending-related CP's mentioned in Sec. IV B. (In this context we draw attention to the discussion in Hass *et al.*,[41] in particular to Fig. 4 therein.) It is gratifying to note that, in a recent

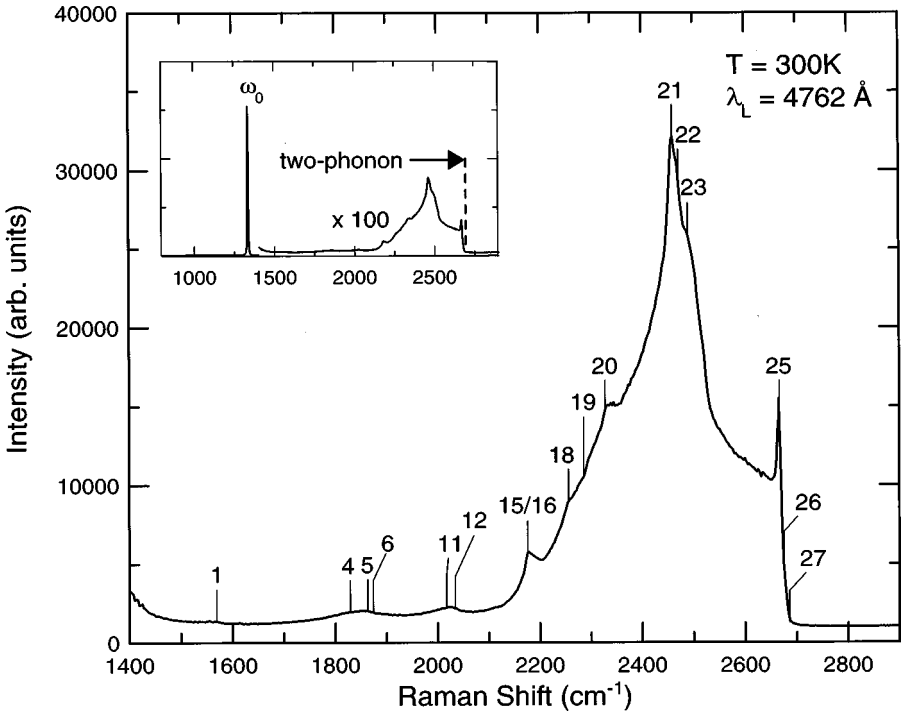

FIG. 2. The Raman spectrum of a natural type-IIb diamond (specimen *D*2), recorded in the backscattering geometry along [111] with the incident light vertically polarized in the (111) plane and the scattered light unanalyzed. This polarization configuration allows the simultaneous observation of the features characterized by the $\Gamma^{(1+)}$, $\Gamma^{(12+)}$, and $\Gamma^{(25+)}$ polarizability tensors. The two-phonon features identified in Table III are explicitly labeled. The inset underscores the relative intensities of the strong $\Gamma^{(25+)}$ zone center optical phonon and the significantly weaker two-phonon features.

TABLE III. Critical point phonon combinations and overtones determined from the present optical data. Along with the wave-vector **q**, the reduction coefficients (Ref. 10) of the product representations are presented, allowing group-theoretical predictions of Raman and IR activity. The last two columns compare the experimental and calculated frequencies based on the present assignments of the spectral features.

No.	**q** $(2\pi/a)$	Assignment	Raman activity $\Gamma^{(1+)}$	$\Gamma^{(12+)}$	$\Gamma^{(25+)}$	IR activity $\Gamma^{(15-)}$	ω (cm^{-1}) Expt.[a]	Calc.
1	(1,0,0)	$[X^{(3)}(\mathrm{TA})]^{(2)}$	1	1	1	0	1569	1572
2	$(\frac{1}{2},\frac{1}{2},\frac{1}{2})$	$L^{(3-)}(\mathrm{TO})\otimes L^{(3+)}(\mathrm{TA})$	0	0	0	2	1780	1780
3	$(\frac{1}{2},\frac{1}{2},\frac{1}{2})$	$L^{(3+)}(\mathrm{TA})\otimes L^{(2-)}(\mathrm{LO})$	0	0	0	1	1817	1817
4	$(1,\frac{1}{2},0)$	$[W^{(2)}(\mathrm{TA})]^{(2)}$	1	1	1	0	1829	1830
5	$\sim 0.78\times(1,1,0)$	$\Sigma^{(2)}(\mathrm{O})\otimes\Sigma^{(4)}(\mathrm{A})$	0	0	1	1	1863	1863
6	(1,0,0)	$X^{(3)}(\mathrm{TA})\otimes X^{(4)}(\mathrm{TO})$	0	1	0	1	1874	1874
7	$(1,\frac{1}{2},0)$	$W^{(1)}(\mathrm{TO})\otimes W^{(2)}(\mathrm{TA})$	0	1	2	2	1927	1927
8	(1,0,0)	$X^{(1)}(\mathrm{L})\otimes X^{(3)}(\mathrm{TA})$	0	0	1	1	1959	1956
9	$\sim 0.75\times(1,1,0)$	$\Sigma^{(1)}(\mathrm{A})\otimes\Sigma^{(3)}(\mathrm{A})$	0	0	1	1	1977	1977
10	$\sim 0.84\times(1,1,0)$	$\Sigma^{(1)}(\mathrm{O})\otimes\Sigma^{(4)}(\mathrm{A})$	0	1	0	1	2007	2007
11	$(\frac{1}{2},\frac{1}{2},\frac{1}{2})$	$[L^{(1+)}(LA)]^{(2)}$	1	0	1	0	2017	2018
12	$\sim 0.70\times(1,1,0)$	$\Sigma^{(3)}(\mathrm{O})\otimes\Sigma^{(3)}(\mathrm{A})$	1	1	1	1	2034	2034
13	$\sim 0.70\times(1,1,0)$	$\Sigma^{(2)}(\mathrm{O})\otimes\Sigma^{(3)}(\mathrm{A})$	0	1	0	1	2095	2096
14	$\sim 0.75\times(1,1,0)$	$\Sigma^{(2)}(\mathrm{O})\otimes\Sigma^{(3)}(\mathrm{O})$	0	1	0	1	2158	2157
15	$(1,\frac{1}{2},0)$	$W^{(1)}(\mathrm{TO})\otimes W^{(2)}(\mathrm{L})$	0	1	2	2	2176	2176
16	(1,0,0)	$[X^{(4)}(\mathrm{TO})]^{(2)}$	1	1	1	0	2176	2176
17	$(\frac{1}{2},\frac{1}{2},\frac{1}{2})$	$L^{(2-)}(\mathrm{LO})\otimes L^{(1+)}(\mathrm{LA})$	0	0	0	1	2254	2254
18	(1,0,0)	$X^{(1)}(\mathrm{L})\otimes X^{(4)}(\mathrm{TO})$	0	0	1	1	2256	2258
19	$\sim 0.73\times(1,1,0)$	$\Sigma^{(1)}(\mathrm{O})\otimes\Sigma^{(3)}(\mathrm{O})$	0	0	1	1	2286	2287
20	$(1,\frac{1}{2},0)$	$[W^{(2)}(\mathrm{L})]^{(2)}$	1	1	1	0	2328	2328
21	$\sim 0.50\times(1,1,0)$	$[\Sigma^{(1)}(\mathrm{O})]^{(2)}$	1	1	1	0	2460	2460
22	$\sim 0.70\times(1,1,0)$	$[\Sigma^{(1)}(\mathrm{O})]^{(2)}$	1	1	1	0	2472	2472
23	$(\frac{1}{2},\frac{1}{2},\frac{1}{2})$	$[L^{(2-)}(\mathrm{LO})]^{(2)}$	1	0	1	0	2490	2490
24	(0,0,0)	High frequency limit of IR active combinations (see text).					2665	2664.8
25	}	''Overbending'' related overtones from				{	2667	
26	}	the topmost optical branch (see text).				{	2676	
27	}					{	2690	

[a]The assignments for features labeled 2, 3, 9–11, 13, 14, 17, 18, 20, 21, and 23 played a significant role in arriving at the phonon frequencies at critical and high-symmetry points.

precision measurement of inelastic neutron scattering from phonons along the Δ_2' line, Kulda *et al.*[42] showed unambiguously that the absolute maximum is not located at Γ.

E. Isotopically controlled diamond

The IR active, two-phonon spectrum of a natural and of a ^{13}C diamond are compared in Fig. 4(a). As can be seen, all the features are reproduced in the two spectra with remarkable fidelity and one can be superimposed on the other nearly perfectly with an appropriate frequency scaling of 0.962 00, as given by the virtual crystal approximation (VCA).[43] In an additional analysis, we obtained ''local'' scaling factors for the vicinities of clearly identifiable features by matching 60 cm^{-1} stretches from the ^{13}C absorption spectrum with the appropriate parts of the natural diamond absorption spectrum. In the range 1800 to 2700 cm^{-1}, we found an average scaling factor of 0.962 01(14) with no apparent dependence on spectral position. Considering the absolute frequency calibration provided by the Fourier transform IR technique, we thus conclude that *the phonon frequencies of the entire BZ do indeed scale with the same VCA-type factor*. This is to be contrasted with the behavior expected for crystal systems composed of two or more different elements, each having its own set of isotopes.[44]

Studied in a similar manner, the two-phonon Raman spectra displayed in Fig. 4(b) again emphasize the excellent correspondence according to the VCA. The ''local'' frequency scaling factors, obtained from matching clear Raman signatures in the range 1300 to 2700 cm^{-1}, showed a standard deviation about 6 times larger than that for the IR spectra, consistent with the somewhat less accurate frequency calibration. As for the IR spectra, an apparently random distribution about the average was observed.

In the light of the possible small departures from VCA, the frequency assignments of Table III for the two-phonon features are restricted to those of the natural composition. We have, however, exploited the improved signal-to-noise (S/N) ratio in several of the ^{13}C Raman spectra [see, for example, Fig. (5)] in *discovering* the CP features.

Zero point motion and anharmonicity are important aspects of the lattice dynamics of diamond.[6] However, even for

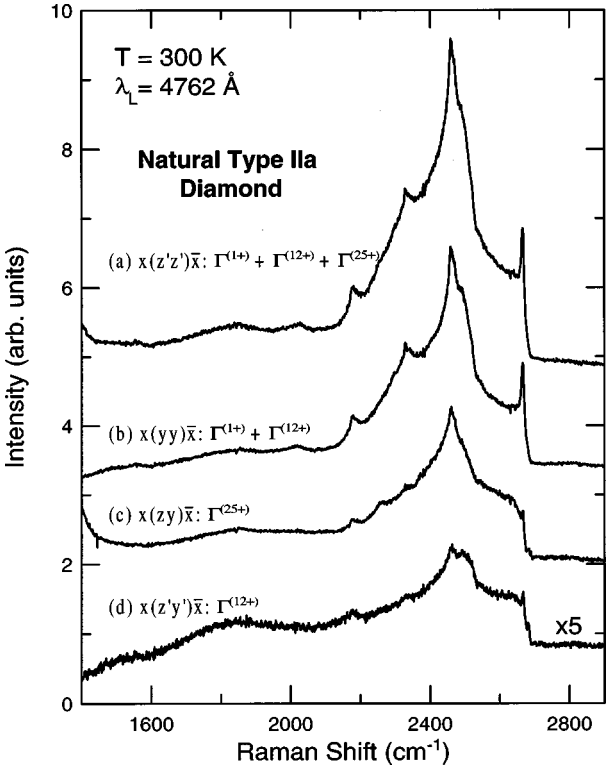

FIG. 3. Polarization effects in the Raman spectrum of a natural type-IIa diamond (specimen $D17$), recorded in the backscattering geometry along $x\|[100]$.

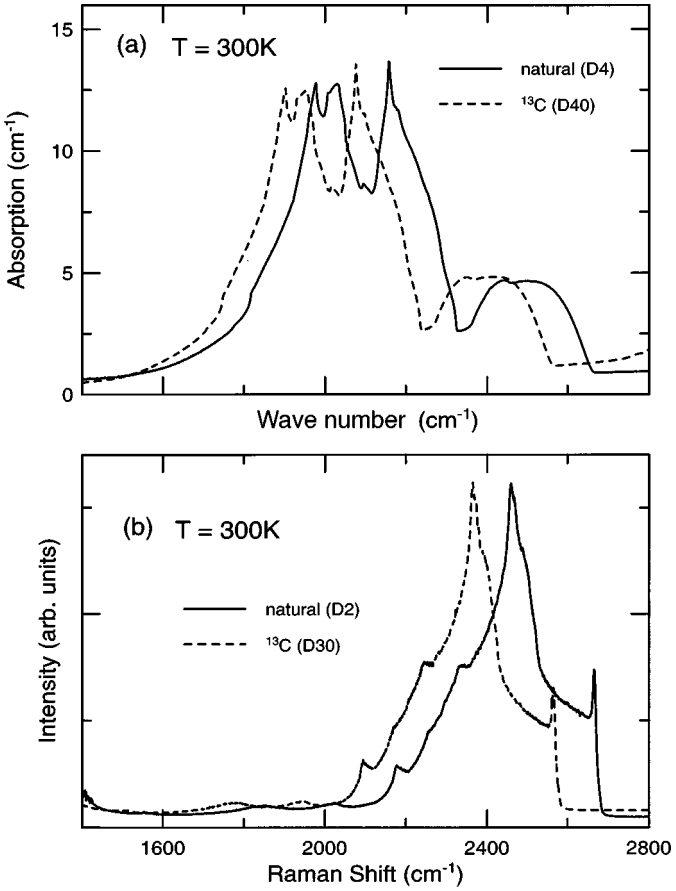

FIG. 4. Effect of isotopic composition on (a) the IR and (b) the Raman spectra of diamond. All the spectral features exhibit a scaling according to $M^{-1/2}$, consistent with the virtual crystal approximation, even to the minutest detail; here M is the average isotopic mass. The properly scaled IR spectrum of $D40$ ($^{12}C_{0.013}{}^{13}C_{0.987}$) in (a) would practically coincide in print with the IR spectrum of $D4$ ($^{12}C_{0.989}{}^{13}C_{0.011}$). The Raman spectra were taken in backscattering geometry along [111].

the single intense line in first order (ω_0), the theoretical prediction is only $\sim 1\ \mathrm{cm}^{-1}$; the lower intensity and superposition of a continuum of states required us to use a lower instrumental resolution, rendering the present spectra less amenable for such an analysis. Hence we must defer the quest for the ''zero-point motion and anharmonicity'' effects in the second-order spectra.

V. CONCLUDING REMARKS

In the present investigation, the superior S/N available in the CCD-based Raman spectrometer and in the Fourier transform IR spectrometer (with mercury cadmium telluride detector and coaddition) has resulted in high quality multiphonon Raman and IR spectra. The data thus acquired reveal the spectral features with improved clarity and yield very reliable, self-consistent interpretations based on critical point analysis, polarization selection, and the Raman and/or IR activity. The assignments as multiphonon combinations or overtones of CP phonons in Table III have led to the CP phonon frequencies listed in Table I. As explained in the text, inelastic neutron-scattering data also provided the discovery of CP's in the two-phonon density of states in the Σ branch as a consequence of Eq. (2).

Since the earlier investigation of the subject of this paper by Solin and Ramdas,[5] much progress has been made in the theory of phonon dispersions. ''Frozen phonon'' calculations[34,35] do not yield the sign and magnitude of the anharmonicity needed to interpret the sharp 2667 cm^{-1} Raman line as due to a ''two-phonon bound state.'' [33] The con-

TABLE IV. Brout sums at various points of the BZ. The last column displays the effect of a nonelectrostatic force acting between second-nearest neighbors.

q ($2\pi/a$)	Neutron (Refs. 1 and 4)	Brout sum (10^6 cm^{-2}) Ref. 5	Present	Eq. (5)
Γ: (0,0,0)		5.3227(40)	5.3259(4)	5.3259
L: $(\frac{1}{2},\frac{1}{2},\frac{1}{2})$	6.15(37)	6.12(6)	6.14(3)	6.13
X: (1,0,0)	6.40(31)	6.40(6)	6.34(3)	6.40
W: $(1,\frac{1}{2},0)$	6.39(50)	6.43(6)	6.43(3)	6.40
Σ: $\sim 0.72\times(1,1,0)$	6.37(25)	6.33(4)	6.36(3)	6.36

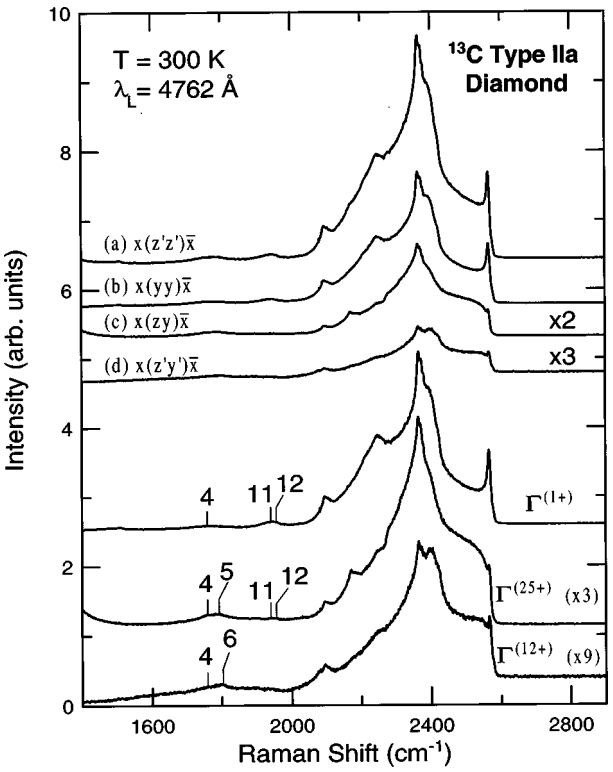

FIG. 5. Polarization effects in the Raman spectrum of a ^{13}C type-IIa diamond (specimen *D*30), recorded in the backscattering geometry along $x\|[100]$ [traces (a)–(d)]. The spectra have been numerically decomposed into the $\Gamma^{(1+)}$, $\Gamma^{(12+)}$, and $\Gamma^{(25+)}$ component spectra based on their contributions to (a)–(d). Features 4–6, 11, and 12 appear with improved clarity in these spectra compared to those in Fig. 3; their positions (with a scaling factor of 1.0395) have been listed in Table III for natural diamond.

jecture that this sharp line arises from the ''overbending'' of the topmost optical branch[24,36,37,39] has been confirmed in the theory of Pavone *et al.*[40] and Windl *et al.*[25]

In the course of the analysis of the two-phonon features in the Raman and IR spectra, we encountered two intriguing examples of coincidences: the maximum in the Raman spectra corresponded to a minimum in the IR, viz. Nos. 20 and 21. The assignments for both are overtone active in Raman but forbidden in IR.

In Table V we list those features that could not be consistently assigned in terms of polarization effects in Raman and IR activity. Since the possibilities for CP's arising from Eq. (2) have not been explored for the entire BZ with the exception of the Σ line, one cannot rule out such assignments in the future. In our assignments for the IR and Raman features associated with the combinations/overtones of the Σ phonons, we paid special attention to the occurrence of CP's on single-phonon branches [e.g., $\Sigma^{(1)}$(O) and $\Sigma^{(3)}$(O) at $\xi \sim 0.72$ and $\Sigma^{(1)}$(O) at $\xi \sim 0.5$] as well as several CP's in the two-phonon density of states as a consequence of Eq. (2).

In a recent study of the IR spectra of CVD diamond films,

TABLE V. Unassigned features in the two-phonon IR and Raman spectra.

Frequency (cm^{-1})	Observed activity $\Gamma^{(1+)}$	$\Gamma^{(12+)}$	$\Gamma^{(25+)}$	$\Gamma^{(15-)}$
2049				1
2054				1
2134				1
2181				1
2298	1			
2360	1	?	1	1
2368	?		1	
2406				1
2466	1	1	1	
2520	1	1	?	

Klein *et al.*[45] have reported features in the one-phonon excitation range, interpreted as ''defect activated'' one-phonon excitations at the CP's due to the relaxation of wave-vector conservation. We have observed the two-phonon spectrum of a single crystal $^{12}C_{1-x}{}^{13}C_x$ ($x=0.47$) diamond (spectra not shown here) and found that the distinct features at $x\sim 1$ and $x\sim 0$ are broadened or lost altogether as a consequence of isotopic disorder. In the CVD films, the one-phonon features presumably arise from a relaxation of translational symmetry due to the grain size of the polycrystalline aggregates and other unavoidable defects. The differences between the assignments of spectral features to the critical points at *X*, *L*, and *W* and the frequencies deduced by them and those derived in the present study have to be viewed in this light. Our discussion of the presence or absence of CP's along Σ becomes particularly relevant in their assignments of defect activated *one-phonon* features to the *K* point of the BZ, i.e., $(\frac{3}{4},\frac{3}{4},0)$. Specifically, the absence of CP's on the $\Sigma^{(4)}$(A), $\Sigma^{(1)}$(A), and $\Sigma^{(2)}$(O) branches rules out several of their assignments. The requirement of self-consistency based on IR activity and presence or absence in the variety of scattering configurations in which the Raman spectra were recorded, all performed with same or similar single bulk crystals, is the underlying basis for our assignments for the spectral features. In this context, the guidance provided by the recent comprehensive calculations (Refs. 25 and 33–41) and the appearance of identical features in natural and ^{13}C diamonds should be underscored.

ACKNOWLEDGMENTS

The work reported in this paper received support from the National Science Foundation (Grant No. DMR 93-03186) at Purdue University and from the U.S. Department of Energy, BES Material Sciences (Grant No. W-31-109-ENG-38) at the Argonne National Laboratory. One of us (A.D.A.) acknowledges support from CNPq, Brazil. We thank D. Strauch and W. Windl for useful discussions.

[1] J. L. Warren, J. L. Yarnell, G. Dolling, and R. A. Cowley, Phys. Rev. **158**, 805 (1967).
[2] W. Hayes and R. Loudon, *Scattering of Light by Crystals* (Wiley, New York, 1978).
[3] H. Z. Cummins and P. E. Schoen, in *Laser Handbook*, edited by F. T. Arecchi and E. O. Schulz-Dubois (North-Holland, Amsterdam, 1972), Vol. 2, p. 1029.
[4] J. L. Warren, R. G. Wenzel, and J. L. Yarnell, *Inelastic Scattering of Neutrons* (International Atomic Energy Agency, Vienna, 1965), Vol. I, p. 361.
[5] S. A. Solin and A. K. Ramdas, Phys. Rev. B **1**, 1687 (1970).
[6] R. Vogelgesang, A. K. Ramdas, S. Rodriguez, M. Grimsditch, and T. R. Anthony, Phys. Rev. B **54**, 3989 (1996).
[7] G. Herzberg, *Molecular Spectra and Molecular Structure: II Infrared and Raman Spectra of Polyatomic Molecules* (Van Nostrand, Princeton, 1945).
[8] L. van Hove, Phys. Rev. **89**, 1189 (1953).
[9] J. C. Phillips, Phys. Rev. **104**, 1263 (1956).
[10] J. L. Birman, Phys. Rev. **127**, 1093 (1962).
[11] J. L. Birman, Phys. Rev. **131**, 1489 (1963).
[12] E. B. Wilson, Jr., J. C. Decius, and P. C. Cross, *Molecular Vibrations* (McGraw-Hill, New York, 1955).
[13] G. F. Koster, J. O. Dimmock, R. G. Wheeler, and H. Statz, *Properties of the Thirty-Two Point Groups* (MIT, Cambridge, 1963).
[14] L. P. Bouckaert, R. Smoluchowski, and E. P. Wigner, Phys. Rev. **50**, 58 (1936).
[15] Type-IIa diamonds are nitrogen-free. The presence of nitrogen produces a large number of impurity related infrared features in the range 7–9 μm; such diamonds are classified as type I.
[16] T. R. Anthony and W. F. Banholzer, Diamond Relat. Mater. **I**, 717 (1992).
[17] H. M. Strong and R. H. Wentorf, Am. J. Phys. **59**, 1005 (1991).
[18] T. R. Anthony, J. C. Bradley, P. J. Horoyski, and M. L. W. Thewalt, Carbon **34**, 1323 (1996).
[19] Spectra-Physics Lasers Inc., 1330 Terra Bella Ave., P.O. Box 7013, Mountain View, CA 94039-7013.
[20] Instruments SA Inc., 3880 Park Ave., Edison, NJ 08820.
[21] UVP Inc., 2066 W. 11th St., Upland, CA 91786.
[22] Bomem, 450 Ave., St. Jean Baptiste, Quebec City, Quebec, Canada G2E 5S5.
[23] T. C. Damen, S. P. S. Porto, and B. Tell, Phys. Rev. **142**, 570 (1966).
[24] K. Uchinokura, T. Sekine, and E. Matsuura, J. Phys. Chem. Solids **35**, 171 (1974).
[25] W. Windl, P. Pavone, K. Karch, O. Schütt, D. Strauch, P. Giannozzi, and S. Baroni, Phys. Rev. B **48**, 3164 (1993).
[26] R. Brout, Phys. Rev. **113**, 43 (1959).
[27] H. B. Rosenstock, in *Lattice Dynamics*, edited by R. F. Wallis (Pergamon, Copenhagen, 1965), p. 205.
[28] H. Bilz, R. Geick, and K. F. Renk, in *Lattice Dynamics* (Ref. 27), p. 355.
[29] G. Nilsson and G. Nelin, Phys. Rev. B **6**, 3777 (1972).
[30] J. M. Calleja, J. Kuhl, and M. Cardona, Phys. Rev. B **17**, 876 (1978).
[31] J. F. Angress and A. J. Maiden, J. Phys. C **4**, 235 (1971).
[32] G. L. Eesley and M. D. Levenson, Opt. Lett. **3**, 178 (1978).
[33] M. H. Cohen and J. Ruvalds, Phys. Rev. Lett. **23**, 1378 (1969).
[34] D. Vanderbilt, S. G. Louie, and M. L. Cohen, Phys. Rev. Lett. **53**, 1477 (1984).
[35] D. Vanderbilt, S. G. Louie, and M. L. Cohen, Phys. Rev. B **33**, 8740 (1986).
[36] S. Go, H. Bilz, and M. Cardona, Phys. Rev. Lett. **34**, 580 (1975).
[37] R. Tubino, L. Piseri, and G. Zerbi, J. Chem. Phys. **56**, 1022 (1972).
[38] R. Tubino and J. L. Birman, Phys. Rev. Lett. **35**, 670 (1975).
[39] R. Tubino and J. L. Birman, Phys. Rev. B **15**, 5843 (1977).
[40] P. Pavone, K. Karch, O. Schütt, W. Windl, D. Strauch, P. Giannozzi, and S. Baroni, Phys. Rev. B **48**, 3156 (1993).
[41] K. C. Hass, M. A. Tamor, T. R. Anthony, and W. F. Banholzer, Phys. Rev. B **45**, 7171 (1992).
[42] J. Kulda, B. Dorner, B. Roessli, H. Sterner, R. Bauer, T. May, K. Karch, P. Pavone, and D. Strauch, Solid State Commun. **99**, 799 (1996). A hint for the existence of such an ''overbending'' can be seen in the neutron data of G. Peckham, *ibid.* **5**, 311 (1967).
[43] A. K. Ramdas, Solid State Commun. **96**, 111 (1995) quotes a simple but rigorous derivation for the $M^{-1/2}$ dependence of the phonon frequencies given by one of us (S.R.).
[44] A. Göbel, T. Ruf, C. T. Lin, M. Cardona, J. C. Merle, and M. Joucla, Phys. Rev. B **56**, 210 (1997).
[45] C. A. Klein, T. M. Hartnett, and C. J. Robinson, Phys. Rev. B **45**, 12 854 (1992).